Journal of Materials Chemistry C

PAPER

View Article Online
View Journal | View Issue

Cite this: J. Mater. Chem. C, 2016, 4, 7622

Strong piezoelectricity in [*H*-β-(2-pyridyl)-Ala-OH][BF_4] and [*H*-β-(2-pyridyl)-Ala-OH][ClO_4] – new amino acid based hybrid crystals†

Maciej Wojtaś,*[a] Anna Gągor[b] and Andrei L. Kholkin[cd]

Received 29th May 2016,
Accepted 14th July 2016

DOI: 10.1039/c6tc02206e

www.rsc.org/MaterialsC

New amino acid based [*H*-β-(2-pyridyl)-Ala-OH][ClO_4] and [*H*-β-(2-pyridyl)-Ala-OH][BF_4] crystals were synthesized and their structure and functional piezoelectric properties were investigated in detail. The former crystallizes in the piezoelectric $P2_12_12_1$ space group whereas the latter belongs to the polar *P*1 space group. Piezoelectric force microscopy (PFM) measurements revealed that the piezoelectric coefficient, d_{15}eff, of the [*H*-β-(2-pyridyl)-Ala-OH][BF_4] crystal is more than twice that in the widely used transducer material lithium niobate, $LiNbO_3$. The crystal structures of both [*H*-β-(2-pyridyl)-Ala-OH] derivatives are characterized by inter- and intramolecular hydrogen bond networks that are responsible for a high piezoresponse. The existence of intramolecular hydrogen bonding was confirmed by means of IR measurements. The thermogravimetric (TGA) technique was applied to study the thermal behavior of the title crystals. The piezoelectric properties are discussed in the context of the crystallographic structure and the microstructure of these crystals.

1 Introduction

Crystalline materials without a centre of inversion are known to exhibit piezoelectric properties (except for the 432 space group). Due to the direct piezoelectric effect, these materials, when subjected to mechanical stress, generate an electric charge proportional to that stress and due to the converse piezoelectric effect they generate mechanical stress when an electric field is applied. This property is widely used in many applications including acoustic transducers, piezomotors or sensors and actuators.[1] An important class of piezoelectrics are ferroelectrics, which exhibit piezoelectric constants significantly higher than those found in nature such as minerals or some bio-organic materials (*e.g.* lamellar-bone, collagen). In this context ferroelectric organic materials are becoming increasingly important because of their potential applications in the areas of microelectronics and micromechanical systems, such as field effect transistors and non-volatile memories.[2,3] Organic compounds are cheaper and their structure can be easily controlled through chemistry as compared to inorganic ferroelectrics/piezoelectrics. The past decade has experienced significant progress in the search for new organic ferroelectrics useful for microelectronics.[1,4,5]

It appears that highly organized molecular dipole assemblies frequently exhibit piezoelectricity due to the presence of polar bonds and natural asymmetry, which is characteristic of many organic biomaterials (proteins, peptides, amino acids and polysaccharides). Furthermore some biomolecules with bias-induced conformational states also possess true ferroelectric properties.[6] One of the most interesting materials for nanoelectronic applications is the alanine derivative, L-phenylalanyl-L-phenylalanine. This material easily self-assembles into tube-like structures.[7] This process that takes place in this dipeptide as well as in L-leucyl-L-leucine, L-leucyl-L-phenylalanine and L-phenylalanyl-L-leucine was studied in detail by Görbitz[8–10] and by Gazit's group.[7,11–14] Later on, Kholkin *et al.*[15] demonstrated that peptide nanotubes (PNTs) are strongly piezoelectric with the orientation of polarization along the tube axis. Recent success in the growth of mm-sized microtubes has allowed study of not only quasistatic piezoelectric properties but also resonance phenomena.[16]

Currently, it seems to be appropriate to widen the current research into organic–inorganic materials, such as amino acid and simple inorganic acid ($HClO_4$, HBF_4, *etc.*) derivatives. Synthesis of such a class of compounds allows us to create an

[a] Faculty of Chemistry, University of Wrocław, 14 Joliot-Curie, 50-383 Wrocław, Poland. E-mail: maciej.wojtas@chem.uni.wroc.pl
[b] W. Trzebiatowski Institute of Low Temperature and Structure Research Polish Academy of Science, PO Box 1410, 50-950 Wrocław, Poland
[c] Department of Physics and CICECO Ű Materials Institute of Aveiro, 3810-193 Aveiro, Portugal
[d] Institute of Natural Sciences, Ural Federal University, 620000 Ekaterinburg, Russia

† Electronic supplementary information (ESI) available. CCDC 1422211, 1447382 and 1447383. For ESI and crystallographic data in CIF or other electronic format see DOI: 10.1039/c6tc02206e

almost unlimited number of new salts with potentially high piezoelectric properties.[17] Moreover, due to the presence of the chiral carbon atom of amino acids (the only exception is glycine) such a material exhibits nonlinear optical (NLO) properties.[18–20] The study of single crystals will allow us to correlate their structure, microstructure and functional piezoelectric properties.

2 Experimental

Hybrid crystals were prepared by reaction of *H*-β-(2-pyridyl)-Ala-OH ((*S*)-2-amino-3-pyridin-2-yl-propionic acid, Bachem) with either tetrafluoroboric acid (50%, POCh) or perchloric acid (60%, POCh) in water solution. The solutions were then dried under ambient conditions and yielded small, colorless, needle-shaped crystals in both cases. The elemental analysis results agreed well with the proposed formulas: [*H*-β-(2-pyridyl)-Ala-OH][BF_4] (hereafter abbreviated as [2PyAla][BF_4], for the tetrafluoroboric derivative): N: 10.82%; C: 37.20%, H: 4.18% (theoretical N: 11.02%; C: 37.83%, H: 4.33%) and [*H*-β-(2-pyridyl)-Ala-OH][ClO_4] (hereafter abbreviated as [2PyAla][ClO_4], for the perchlorate derivative): N: 10.36%; C: 35.91%, H: 3.47% (theoretical N: 10.50%; C: 36.04%, H: 4.13%). The samples for the AFM measurements were prepared by drying a drop of the water solution of [2PyAla][BF_4] or [2PyAla]-[ClO_4] on a platinum coated silicon substrate.

Thermogravimetric analyses (TGA) and differential thermal analyses (DTA) were performed on a Setaram SETSYS 16/18 instrument in a nitrogen atmosphere in the temperature range 298–900 K and at a 5 deg min^{-1} heating rate for both samples. [2PyAla][BF_4] sample mass: 16.721 mg; [2PyAla][ClO_4] sample mass: 9.1395 mg.

The PFM measurements were performed using a commercial AFM (Ntegra Prima, NT-MDT) equipped with an external function generator and a lock-in amplifier (see ref. 22 for more details). We used doped Si cantilevers with spring constants in the range of 0.35–6.1 N m^{-1} driven by an AC voltage of 5 V peak-to-peak at a frequency of 100 kHz.

Optical microscope observations were carried out by means of a Zeiss Axioplan 2 optical microscope equipped with a Zeiss AxioCam ICc.

Crystal data, data collection and structure refinement details are summarized in Table 1. Experiments were carried out at 298 K with Mo Kα radiation using an Xcalibur, Sapphire1, long nozzle diffractometer. Data were collected in ω-scan mode with $\Delta\omega = 1.0^\circ$ using the CrysAlisCCD programme.[23] CrysAlisPRO was used for data processing.[24] Empirical absorption correction was performed using spherical harmonics, implemented in CrysAlisPRO. The structure was solved by direct methods and refined by the full-matrix least-squares method against F^2 by means of SHELXL2014/7.[25] H atoms were treated by a mixture of independent and constrained refinement. The donor H atoms from NH_3 as well as NH groups have been refined with constraints because of their proximity to librating perchlorate and BF_4^- ions. Rigid body constraints were applied to disordered

Table 1 Crystal data, experimental details and structure refinement results for [2PyAla][BF_4] and [2PyAla][ClO_4] crystals

	[2PyAla][ClO_4]	[2PyAla][BF_4]
Crystal data		
Chemical formula	$C_8H_{11}ClN_2O_6$	$C_8H_{11}BF_4N_2O_2$
M_r	266.64	254.00
Crystal system, space group	Orthorhombic, $P2_12_12_1$	Triclinic, $P1$
a, b, c (Å)	5.3294(2), 10.3097(5), 19.222(1)	5.0586(2), 9.4971(4), 11.2012(5)
α, β, γ (°)	90, 90, 90	87.637(4), 80.166(3), 89.255(3)
V (Å^3)	1056.13(8)	529.76(4)
Z	4	2
F(000)	548	260
μ (mm^{-1})	0.38	0.16
Colour	Colourless	Colourless
Crystal size (mm)	0.3 × 0.15 × 0.09	0.25 × 0.21 × 0.15
Data collection		
T_{min}, T_{max}	0.779, 1.000	0.989, 1.000
No. of measured, independent and observed [$I > 2\sigma(I)$] reflections	3851, 2004, 1674	5209, 3441, 3003
R_{int}	0.02	0.018
q values (°)	q_{max} = 25.7, q_{min} = 2.9	q_{max} = 25.7, q_{min} = 2.8
$(\sin q/l)_{max}$ (Å^{-1})	0.61	0.61
Completeness to q_{max} (%)	99.8	99.4
Refinement		
$R[F^2 > 2\sigma(F^2)]$, $wR(F^2)$, S	0.033, 0.083, 0.85	0.050, 0.121, 1.01
No. of reflections	2004	3441
No. of parameters	158	391
No. of restraints	0	175
$D\rho_{max}$, $D\rho_{min}$ (e Å^{-3})	0.25, −0.25	0.29, −0.22
Absolute structure	Flack × determined using 578 quotients $[(I+) - (I-)]/[(I+) + (I-)]$[21]	Refined as an inversion twin.
Absolute structural parameter	−0.02(3)	The crystal is a weak anomalous scatterer

BF_4^-. Additional data collection was performed at 100 K for [2PyAla][BF_4] to validate the structure solution at room temperature that was performed in the presence of a vast thermal disorder of BF_4. The results are presented in an additional cif file attached as the ESI.† The low temperature refinement confirmed the correct solution of the room temperature structure. The latter was used for the discussion and comparison of the crystallographic details of [2PyAla][ClO_4] and [2PyAla][BF_4] measured under the same conditions. CCDC 1422211, 1447382 and 1447383 contain the crystal information data file for the structure of [2PyAla][ClO_4], [2PyAla][BF_4] (RT) and [2PyAla][BF_4] (100 K), respectively.

3 Crystal structure

3.1 The crystal structure of [*H*-β-(2-pyridyl)-Ala-OH][ClO_4]

[*H*-β-(2-Pyridyl)-Ala-OH][ClO_4] crystallizes in the orthorhombic system, in the chiral space group $P2_12_12_1$. This molecular salt consists of ClO_4^- anions and protonated 3-(2-pyridyl)alanine counterions. The asymmetric unit is built of one ClO_4^- and one 3-(2-pyridyl)alanine counterion, both of C_1 symmetry, see Fig. 1(a). The Cl–O distances range from 1.417(3) to 1.427(3) Å whereas the O–Cl–O angles from 108.8(2)° to 110.9(1)° indicate a small distortion from the ideal tetrahedral arrangement. Elongated displacement ellipsoids come from the temperature induced libration motions of perchlorate.

There are two protonation sites in the counterion: the amine group and the nitrogen from the pyridine ring. The first site is verified by the distance between the α-carbon and the amine nitrogen atom C(2)–N(1) of 1.481(4) Å that is characteristic of a single bond and indicates that the amine group is protonated. The latter one is validated through the C(5)–N(2)–C(4) angle of 122.6° in the pyridine ring that points to protonation of the ring nitrogen N(2). Additionally, the C–O bonds of the carboxylate group are double with lengths less than 1.252(4) Å that support the appropriate location of protonation centers. The carboxyl group is bent towards the pyridinium ring (the C(3)–C(2)–C(1)–O(6) dihedral angle is equal to −59.7(1)°). This conformation promotes the formation of an intramolecular hydrogen bond N(2)–H···O(6) with a donor to acceptor distance of 2.623(4) Å and a donor to acceptor angle equal to 167(3)°.

The supramolecular assembly is controlled by numerous hydrogen bonds between the amine hydrogen atoms, CH_2, CH groups and ClO_4^- anions. N–H···O, O–H···O and C–H···O intermolecular interactions are crucial in building supramolecular architectures in organic–inorganic hybrids as well as metal–organic materials.[26–28] Oxygen from perchlorate ions acts as an acceptor in 7 different hydrogen bonds. Table 2 summarizes the hydrogen bond parameters whereas Fig. 2(a) and (b) illustrates the crystal packing and hydrogen bonds in the crystal structure of [2PyAla][ClO_4]. The strongest hydrogen bonds are formed between the protonated 3-(2-pyridyl)alanines.

Table 2 Selected hydrogen-bond parameters

D–H···A	D–H (Å)	H···A (Å)	D···A (Å)	D–H···A (°)
[2PyAla][ClO_4]				
N1–H1A···O4^{i}	0.89	2.04	2.926(4)	170.4
N1–H1B···O5^{ii}	0.89	1.89	2.771(4)	171.5
N1–H1C···O2	0.89	2.1	2.965(4)	162.9
N2–H9···O6	0.91(4)	1.73(4)	2.623(4)	167(3)
C3–H3A···O3^{ii}	0.97	2.49	3.444(5)	166.8
C3–H3B···O3	0.97	2.59	3.500(5)	156.4
C6–H6···O2^{iii}	0.93	2.54	3.264(5)	135.2
C6–H6···O4^{iv}	0.93	2.59	3.211(5)	124.4
C8–H8···O1^{v}	0.93	2.53	3.347(5)	147.4
[2PyAla][BF_4]				
N28–H28···O12	0.86	1.81	2.636 (6)	159.3
N27–H27···F3	0.86	2.01	2.747 (14)	142.8
N27–H27···F3′	0.86	1.99	2.829 (9)	163.2
N15–H15A···F6^{vi}	0.89	2.28	2.967 (9)	134.2
N15–H15A···F7	0.89	2.31	2.934 (10)	127.1
N15–H15A···F6′^{vi}	0.89	2.42	3.063 (14)	129.2
N15–H15A···F7′	0.89	2.12	2.849 (17)	138.8
N15–H15B···O12	0.89	1.88	2.762 (5)	172.2
N15–H15C···O17^{vii}	0.89	1.97	2.816 (5)	157.1
N14–H14A···F4^{viii}	0.89	2.29	2.856 (16)	121
N14–H14A···F1′^{ix}	0.89	2.27	2.790 (11)	117
N14–H14A···F2′^{viii}	0.89	2.27	3.081 (10)	150.5
N14–H14B···O17^{ix}	0.89	1.87	2.743 (5)	167.7
N14–H14C···O16^{viii}	0.89	2.04	2.826 (5)	146.8

Symmetry codes: (i) $x+1/2, -y+1/2, -z+2$; (ii) $x+1, y, z$; (iii) $x, y-1, z$; (iv) $x+1, y-1, z$; (v) $-x+2, y-1/2, -z+3/2$. (vi) $x+1, y, z$; (vii) $x-1, y, z$; (viii) $x, y-1, z$; (ix) $x-1, y-1, z$.

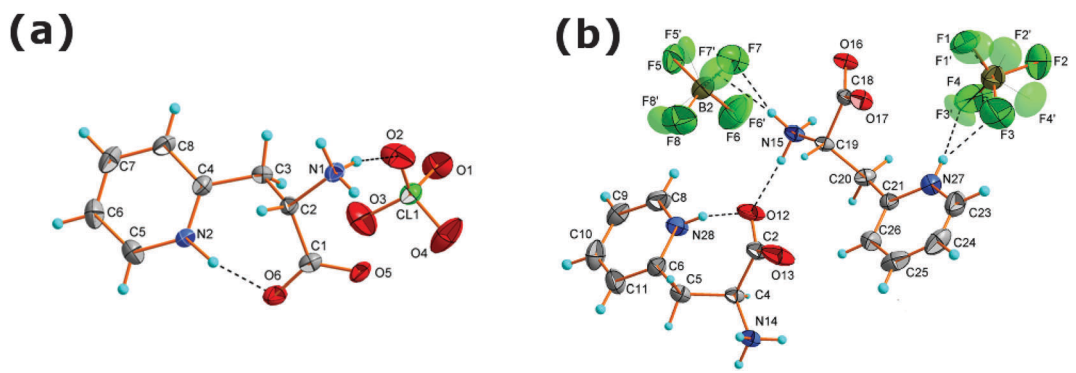

Fig. 1 The content of the asymmetric unit of [2PyAla][ClO_4] (a) and [2PyAla][BF_4] (b) together with the atom numbering scheme. Dashed lines indicate hydrogen bonds. BF_4^- ions are dynamically disordered. Displacement ellipsoids are drawn with 50% probability.

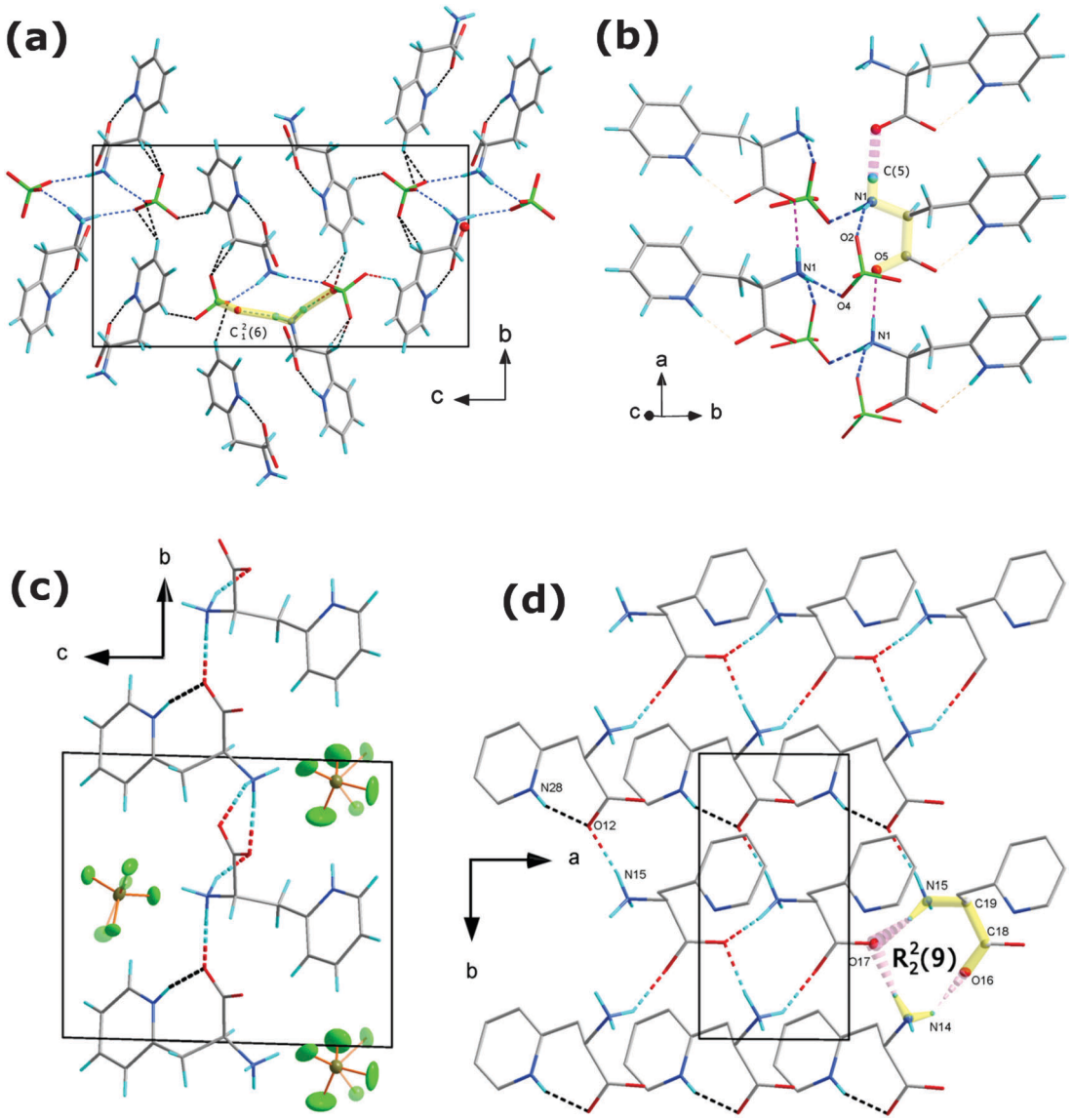

Fig. 2 (a) Crystal structure packing of [2PyAla][ClO_4] as seen along the *a* direction; N–H···O and C–H···O hydrogen bonds form extended 3D supramolecular structure. $C_1^2(6)$ synthon is marked by thick yellow lines; (b) selected hydrogen bonds in [2PyAla][ClO_4], intermolecular interactions are bolded, C(5) synthon is marked by thick pink-yellow lines. (c) Packing of the crystal structure of [2PyAla][BF_4]; (d) the hydrogen bonded [2PyAla]$^+$ 2D layers of [2PyAla][BF_4]. The elemental R ring motif is marked in yellow and pink. Hydrogen bonds are represented as dashed lines. Hydrogen atoms not involved in bonding have been omitted for picture clarity.

They involve an amine hydrogen atom and an oxygen atom from the carboxylic group. The N1–H···O5 bonds connect neighboring cations in the *a* direction forming infinite chains built of the C(5) motif,[29] see Fig. 2(b). Strong hydrogen bonds are also found between the protonated 3-(2-pyridyl)alanine and perchlorate oxygen atoms. They form spiral chains which propagate along the *a* direction and may be described by the $C_1^2(6)$ synthon. There are two N1–H···O4 and N1–H···O2 bonds within the motif, formed between the NH_3 group of protonated 3-(2-pyridyl)alanine and two perchlorate anions. The weak C–H···O contacts with donor to acceptor distances ranging from 3.211(5) to 3.444(5) Å also stabilize the supramolecular structure although the bonding strength of sp^2 and sp^1 carbons is weaker (see ref. 30 and references therein).

3.2 The crystal structure of [*H*-β-(2-pyridyl)-Ala-OH][BF_4]

[*H*-β-(2-Pyridyl)-Ala-OH][BF_4] crystallizes in the triclinic system with *P*1 symmetry. The asymmetric unit presented in Fig. 1 consists of two independent protonated 3-(2-pyridyl)alanine cations A and B and two BF_4^- groups. Both BF_4^- anions are disordered and occupy two inequivalent positions with 0.36(1)/0.64(1) and 0.37(2)/0.63(2) probabilities at room temperature. This, together with large anisotropic displacement parameters, implies that the whole anions are thermally disordered and may perform rotational motions around the gravity center (positions of the borate atoms). The disorder remains after cooling to 100 K though the site occupancy changes to 0.26(1)/0.74(1) and 0.58(4)/0.42(4), respectively. The 3-(2-pyridyl)alanine is protonated as in

[2PyAla][ClO_4]. The C(4)–N(14) and C(15)–N(19) distances are 1.495(6) and 1.481(6) Å which are characteristic of single N–C bonds and indicate the protonation of amine groups. Similar to [2PyAla][ClO_4], ring nitrogen atoms are protonated at both independent counterions with C(21)–N(22)–C(23) and C(8)–N(28)–C(6) angles of 122(1)° and 123(1)°, respectively. The C–O bond lengths in the carboxylate groups range from 1.226(6) to 1.256(6) Å which are typical of double bonds.

The conformation of A and B counterions is different. In A, similar to [2PyAla][ClO_4] the carboxylate group is bent towards the pyridinium ring and an intramolecular N(28)–H···O(12) hydrogen bond is formed with a ring nitrogen serving as a donor and oxygen from the carboxylate group as an acceptor. The donor to acceptor distance equals 2.636(6) Å, and the donor to acceptor angle equals 159°. In B the side chain is more straightened and the carboxylate group is directed towards amine NH_3 from neighboring A counterions forming strong intramolecular hydrogen bonds with amine hydrogens, see Fig. 2(c) and Table 2. In [2PyAla][BF_4] the strongest hydrogen bonds are formed between the 3-(2-pyridyl)alanines, between amine hydrogen atoms and oxygen from carboxylate groups. The donor to acceptor distances range from 2.743(5) to 2.826(5) Å and the angles range from 147 to 172°. They form 2D layers expanding in the *a* and *b* directions. Among them, along with the intramolecular bond and N(15)–H···O(12) bonds the ring motifs may be recognized with two donor and two acceptor atoms ($R_2^2(9)$). The supramolecular structure is also stabilized, especially in the *c* direction, by numerous N–H···F interactions (see Fig. 2(d)), which are listed in Table 2. Due to the pronounced vibration motions of BF_4^- groups these hydrogen bonds are less stable.

4 IR measurements

Fig. 3(a) and (b) shows the IR spectra of [2PyAla][ClO_4] and [2PyAla][BF_4], respectively, recorded in fluorolube and nujol oil under ambient conditions. Both spectra are characterized by broad, intense absorption forming a continuum resembling a Hadži's trio.[31] It can be fit well with 3 components with the peak maximum at 2780 cm^{-1}, 1480 cm^{-1} and 1000 cm^{-1} in the case of [2PyAla][ClO_4] and 2900 cm^{-1}, 1500 cm^{-1} and 990 cm^{-1} for [2PyAla][BF_4]. In both cases the observed images fit the asymmetric potential with a double minimum for hydrogen motion. This potential may be described using the formula:[32]

$$V(r,R) = a_2(R)r^2 + a_3(R)r^3 + a_4(R)r^4,$$

where *r* stands for the coordinate of the proton movement, *R* is the coordinate of the hydrogen bridge vibration and a_2, a_3 and a_4 are *R* dependent parameters. The observed profiles of the trio components are caused by the coupling of the anharmonic stretching vibrations of the proton of the hydrogen bond with the hydrogen bridge vibrations, which are damped by interactions with the lattice phonons.[33] It should be emphasized that the results of IR measurements totally agree with the X-ray finding of strong, intramolecular hydrogen bonds.

Table 3 presents the band frequencies and their assignments. The assignments reported in ref. 34–36 were used as guides.

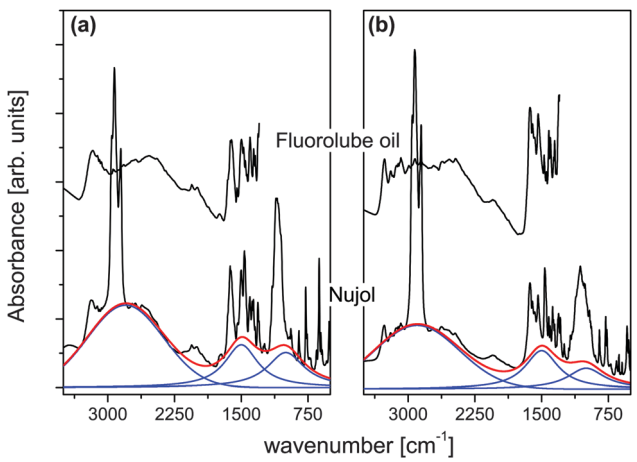

Fig. 3 Infrared spectra of [2PyAla][ClO_4] (a) and [2PyAla][BF_4] (b) in nujol and fluorolube oil.

5 Thermal behavior

Fig. 4 presents the results of thermogravimetric (TGA) measurements of the [2PyAla][BF_4] (a) and [2PyAla][ClO_4] (b) samples. Both crystals are thermally stable up to *ca.* 453 K ([2PyAla][BF_4]) and 459 K ([2PyAla][ClO_4]). At these temperatures the decomposition of the salts starts and up to 875 K both crystals lose about one third of the initial mass. It should be added that using the differential scanning calorimetry (DSC) technique we did not find any other phase transition in the temperature range 100–450 K. Though the thermal behavior of both studied crystals is very similar it is worth noting that the decomposition of the [2PyAla][ClO_4] sample is linked to an additional thermal anomaly manifested as an exoenergetic peak (at *ca.* 590 K). Such an effect is, however, common for perchlorate derivatives.[37,38]

6 PFM measurements

Fig. 5(a) presents the optical microscopy (magnification 5×) image of the [2PyAla][BF_4] sample. One can see the elongated, either needle or plate shaped, crystals. The AFM images (Fig. 5(b) and (c)) were acquired in a contact mode and the topography and out-of-plane (OOP) piezoresponse signals were recorded simultaneously (PFM – piezoresponse force microscopy, for more details see ref. 39). Fig. 5(d) shows the cross-section of the topography and piezoresponse signals of the sample taken along the lines marked in the corresponding AFM and PFM images. The dotted line intersecting the graph is the piezoresponse 0 value. It is clearly visible that the topography of the sample is strongly correlated with the piezoresponse and the microcrystals exhibit a positive (the crystal on the left) or negative signal. It is worth noting that the absolute piezoresponse either positive or negative is practically the same.

Fig. 5(e) shows the image of the [2PyAla][ClO_4] sample recorded by means of an optical microscope. The majority of

Table 3 Vibrational frequencies of [*H*-β-(2-pyridyl)-Ala-OH][BF_4] and [*H*-β-(2-pyridyl)-Ala-OH][ClO_4] in nujol and fluorolube oil recorded under ambient conditions

BF_4	ClO_4	
Wavenumbers [cm^{-1}]	Wavenumbers [cm^{-1}]	Assignments
3268m,3265s^{f}		
3194vw,3195m^{f}	3184m,3169m^{f}	Asym. NH_2 stretch.
3138w^{f}	3116vw,3113w^{f}	Aym. NH_2 stretch.
3082w,3082w^{f}	3095w^{f},3307vw,3068w^{f}	Asym. NH_3 stretch., C–H aromatic
2990vw^{f}	3019vw^{f}	
2953^{n},2926^{n},2923w^{f}	2968^{n},2941w^{f},2936^{n}	
2869sh^{n},2853w^{f},2822w^{f}	2925vw^{f},2901,2849w^{f}	
2854^{n},2723w	2878,2822w^{f},2861^{n}	
	2722vw,2693vw,2680w^{f}	
2626w,2614w^{f}	2617vw	NH stretch. in NH_3
2538vw,sh,2538w^{f},2470w	2538vw,sh,2535w^{f},2448w^{f}	
2467w^{f}	2445w	
	2347vw^{f}	Stretch. CNH bend.
2051m,2049w^{f}	2145vw^{f},2057w^{f},2056vw	
1995w^{f},1870vw,1869vw^{f}	1997vw,1995w^{f},1866vw^{f}	
1743vw^{f}	1744w^{f},1725w	
	1655sh,1654sh^{f}	NH_2 bend.
1631s,1630vs^{f},1603m	1626s,1626vs^{f},1610vs^{f}	C═N conjugated
1602s^{f}		
1575w^{f},1574w		
1540s,1539vs^{f}	1548m^{f},1541w	NH_3 puckering
	1501s,1498vs^{f}	C═C and C═N conjugated
1472m^{f},1465s^{n},1446w^{f}	1474m^{f},1466s^{n},1454m^{f}	CH_2 bend.
1420m,1419s^{f},1403m	1437w^{f},1404m,1401s^{f}	
1402s^{f}		
1377m^{n}	1377m^{n}	CH_3 bend.
1365m^{f},1364w,1355w	1364m,1361m^{f}	NH_3 puckering
1354m^{f},1335m^{f}	1345w,1343m^{f}	
1310s	1313s	CN stretch.
1290m,1194w,1194w	1299m,1248w,1239w	
1177m		
1150w	1150w	NH bend.
1121sh		
1065vs	1110vs,1094vs,1082vs	H_3–N_1–C_2–C_3 bend.
	1047s,sh	
1013w	1004vw	Asym NC_2 stretch.
898w,851s	853m	Sym. NC_2 stretch.
780s	776s	NH_2 rocking
767s^{n}	760m^{n}	CCH bend.
736w,722w	736w,720w	HNC bend.
659m	653m	OCOH + NH_2 bend.
630s,608w,596m	625s,605m,592w	
540vs	540w	OH bend.
522s,496m,479m	513m,480w	

n – bands of nujol oil; f – bands observed in fluorolube oil. vs – very strong; s – strong; m – medium; w – weak; vw – very weak; and sh – shoulder.

the microcrystals are needle shaped, elongated along *a*. The cross section of the crystals is rectangular and two other crystallographic directions, *b* and *c*, are normal to surfaces parallel to *a* – see Fig. S1 in the ESI.† Fig. 5(f) presents a selected microcrystal and its piezoresponse (part (g)) recorded in the plane (IP, the bottom part of the image) and OOP (the upper part of the image). The difference is striking, and one may observe only a residual OOP signal. Its magnitude is non-zero which seems to be caused by the concretion of the crystals with different orientation of molecules. The diagram below presents the piezoelectric coefficient matrix for point group 222 according to Nye.[40]

$$\begin{pmatrix} \cdot & \cdot & \cdot & d_{14} & \cdot & \cdot \\ \cdot & \cdot & \cdot & \cdot & d_{25} & \cdot \\ \cdot & \cdot & \cdot & \cdot & \cdot & d_{36} \end{pmatrix}$$

In crystals belonging to the 222 point group the piezoresponse has its origin only in shear deformations. Since the concreted parts of crystals are elongated along *a* the OOP signal may derive either from d_{25} if the electric field is parallel to *b* or from d_{36} if the electric field is parallel to *c*. It is worth noting that a similar observation was made in the case of pure amino-acid crystals of *H*-β-(2-pyridyl)-Ala-OH.[41] It seems that the way of preparation of the sample on the substrate (see the Experimental section) may lead to the growth of non-uniform microcrystals.

In order to prove the piezoelectric character and estimate the magnitude of this effect the piezoresponse *vs.* AC electric field measurements were carried out. However, due to the inhomogeneous E-field distribution[42] the PFM gives only the effective piezoresponse. Thus the results of the [2PyAla][BF_4] and [2PyAla][ClO_4] piezoresponse were compared to those of a

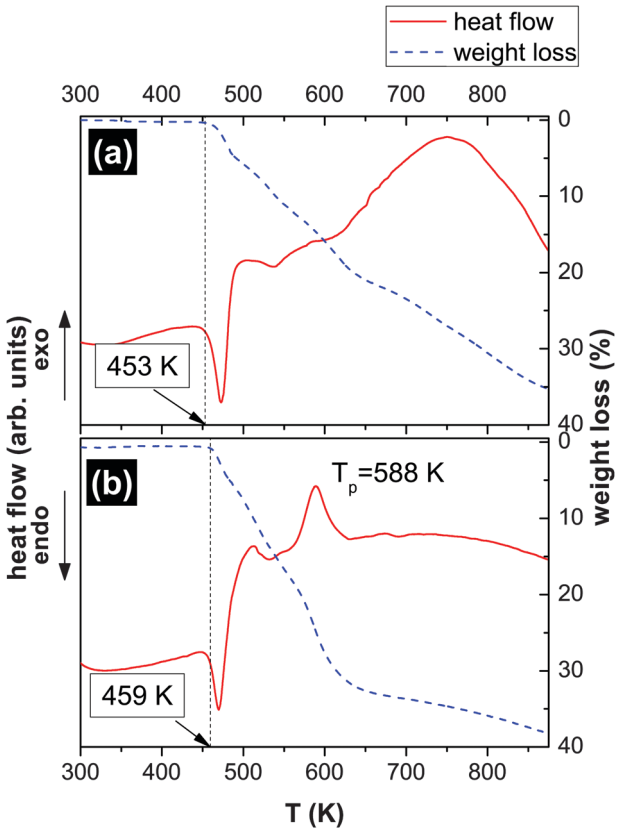

Fig. 4 TGA scans of [2PyAla][BF_4] and [2PyAla][ClO_4]. The scans were performed in flowing nitrogen with a ramp rate of 5 deg min^{-1}. The vertical dashed line shows the onset point of the peak in the DTA curve and the beginning of the corresponding mass loss of the sample.

commercially available $LiNbO_3$ (LNO) sample (periodically poled lithium niobate, cut normal to the polar axis, NT-MDT). In this way it is possible to quantify the piezoeffect in various materials avoiding rigorous calculations.[43] Fig. 6 shows the out-of-plane and in-plane piezoresponse signals of [2PyAla][BF_4] and the in-plane signal of [2PyAla][ClO_4] crystals in comparison with the LNO out-of-plane signal (d_{33} = 17 pm V^{-1} – see Wong[44]). In the case of the titled crystals the estimated piezoelectric coefficients were labelled 'eff' since the piezoresponse of perchlorate and tetrafluoroborate derivatives is a function of shear ([2PyAla][ClO_4]) and the shear and extension ([2PyAla][BF_4]) components, respectively. It is also the reason that the most striking feature is the fact that the piezoresponse of the IP signal of [2PyAla][BF_4] is twice as high as that of the LNO sample. It should be noted that the recorded piezoresponse is very stable and both titled crystals can be driven under a high excitation level since neither nonlinearity nor irreversibility even at an AC voltage of 20 V was observed. The OOP response of perchlorate crystals was insignificant and was not presented in the graph.

7 Discussion

7.1 [*H*-β-(2-Pyridyl)-Ala-OH][ClO_4]

[2PyAla][ClO_4] is a new peptide-based crystal. Since it crystallizes in the $P2_12_12_1$ space group it is a piezoelectric material. This is another amino acid derivative adopting the space group which is by far the most commonly observed crystal space group for (ordinary chiral) proteins.[45,46] One of the most interesting features besides the piezoelectricity is the spiral chains which comprise ClO_4^- oxygen atoms and protonated amino group N atoms interacting *via* hydrogen bonds (see Fig. 7). This arrangement resembles to some extent the structure observed in the case of L-Leu-L-Leu (LL), L-Leu-L-Phe (LF), L-Phe-L-Leu (FL), and L-Phe-L-Phe (FF).[8] The cross-section of the channel of [2PyAla][ClO_4] is a rectangle of dimensions *ca.* 5.5 × 3.5 $Å^2$, whereas the diameter of each rod (LL, FL and FF) could be roughly estimated to be in the range 17–24 Å. It was shown that the cyclic decapeptide *cyclo*[-(L-Trp-D-Leu)$_4$-L-Gln-D-Leu-] with a 10 Å pore size (diameter) can transport glucose efficiently[47] and dynamic transport of various species was expected in the case of the above mentioned dipeptides. The channels existing in the title crystal seem to be too narrow to act as tunnels to transport other molecules but, like in the case of *H*-β-(2-pyridyl)-Ala-OH[41] other molecules may be expected to be incorporated into the [2PyAla][ClO_4] crystal as inclusions.

7.2 [*H*-β-(2-Pyridyl)-Ala-OH][BF_4]

[2PyAla][BF_4] crystallizes in the polar *P*1 space group. The most interesting feature of this crystal is its piezoelectricity. The out-of-plane piezoelectric coefficient of the crystal response is very similar to that observed in $LiNbO_3$, but the piezoelectric coefficient registered in-plane is over twice as high. This finding situates this crystal at the top of organic, amino acid based materials taking into account piezoelectric properties.

The question as to why two compounds of very similar composition crystallize in two different crystallographic systems and therefore different space groups remains open. The crystal structure of salts of amino acid and their properties depend on many factors, such as: the charge state and conformation of the cation, the structure, composition and dynamical state of the anion as well as the hydrogen bond system.[48] In the case of the title crystals one may suggest that the key feature is the disorder of the anions – in the [2PyAla][BF_4] the anions are disordered down to 100 K, whereas the $[ClO_4]^-$ anions exhibit different dynamic states and the disorder is much less significant. It must however be remembered that this model is a bit speculative since [2PyAla][BF_4] and [2PyAla][ClO_4] are the first derivatives of [*H*-β-(2-pyridyl)-Ala-OH] with inorganic acids. In the case of L-arginine and L-histidine, Petrosyan[49] points out 9 different formation mechanisms on the basis of structural analysis of more than 80 salts of these amino acids. Among the salts of L-arginine there are compounds which crystallize either in the orthorhombic system (space group $P2_12_12_1$) like *e.g.* (L-ArgH)ClO_4[50] or in the monoclinic system ($P2_1$) like *e.g.* (L-$ArgH_2$)$(NO_3)_2$[51] or triclinic (*P*1) like *e.g.* (L-$ArgH_2$)$(ClO_4)_2$.[17] Another factor affecting the symmetry of the title crystals might be the strength of the acid and its influence on the charge state of the amino acid. Perchloric acid is considered as one of the strongest acids with a pK_a of the order of −8 whereas tetrafluoroboric acid's pK_a is −4.9 (see ref. 52) thus both acids are very strong. The hypothesis that $HClO_4$ fixes the structure stronger and the piezoresponse is lower than in the HBF_4 derivative is also speculative. Most probably the hydrogen

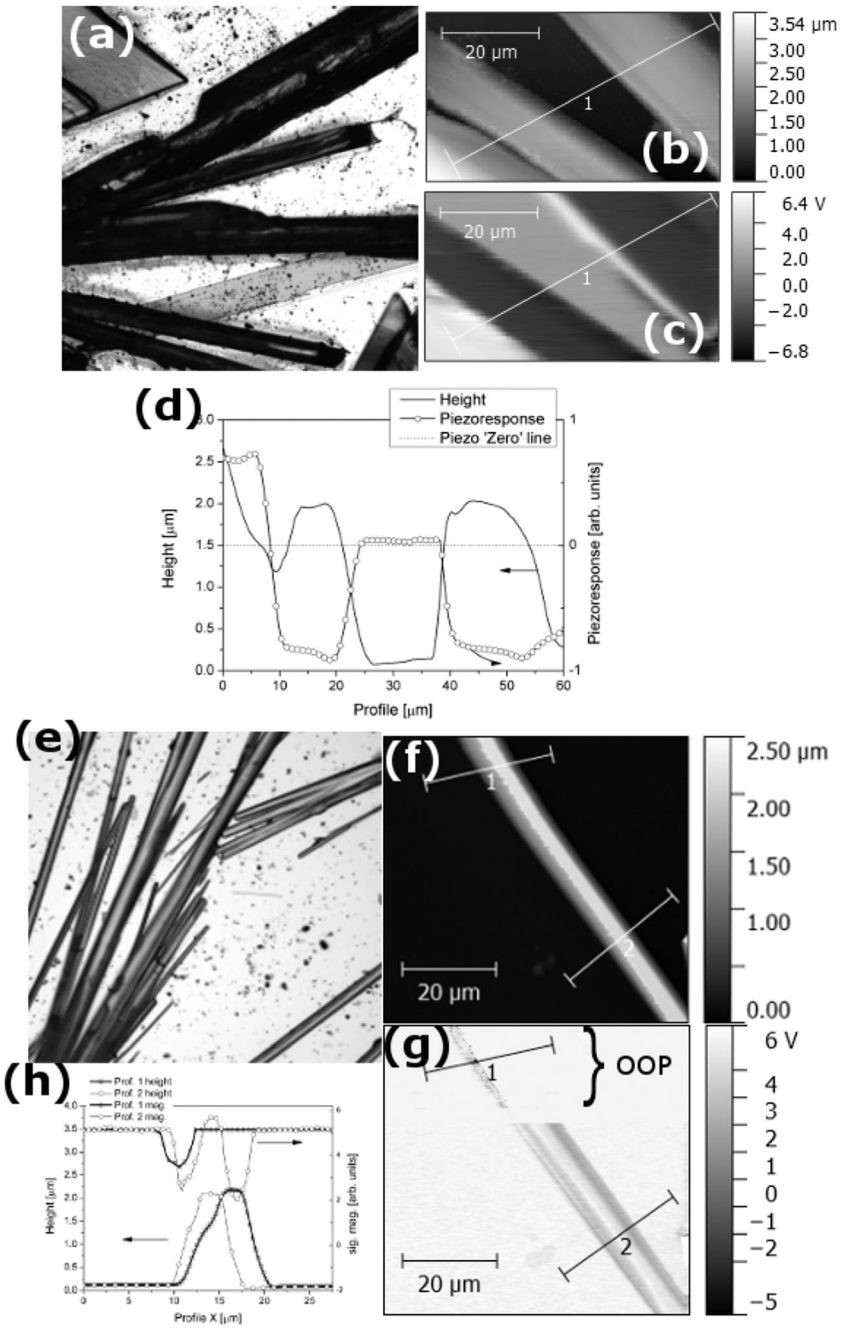

Fig. 5 (a) The optical microscopy image of [2PyAla][BF_4] taken with magnification 5×, (b) topography and piezoresponse (c) of the [2PyAla][BF_4] sample and (d) profile graph along line 1. The dotted line intersecting the graph indicates the piezoresponse 0 value. (e) The optical microscopy image of [2PyAla][ClO_4] taken with magnification 5×, (f) topography and piezoresponse (g) of the [2PyAla][ClO_4] sample and (h) profile graph along lines 1 and 2.

bond network is crucial but the strict correlation between the hydrogen bonds and the structure remains unknown – see for example Görbitz[8] or Surekha *et al.*[20] It is worth noting that introduction to the building compounds of heterocyclic rings makes the hydrogen bond network stabilizing the building units more extensive. This, in turn, may produce polar properties and lead to the emergence of ferroelectricity[53] in those amino acid derivatives. It should be added that there are some recent applications based on piezoelectricity where H-bonding plays a significant role, see for instance Garain *et al.*,[54] Jana *et al.*,[55] Alam and Mandal[56] or Tamang *et al.*[57]

It seems to be very promising to substitute the tetrafluoroboric or perchlorate anions either completely or partly by other inorganic anions. The number of such exchange possibilities is almost unlimited and some of them, with a high degree of possibility, may lead to crystals with desired properties – both piezoelectric and suitable for biomedical applications. The latter may be realized by using the material as a media for

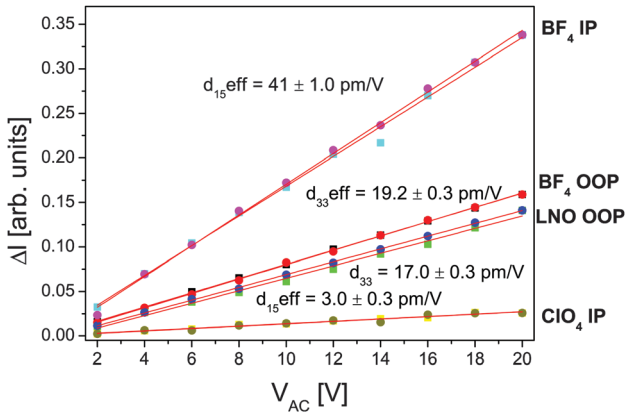

Fig. 6 AC voltage dependencies of IP and OOP displacements of [2PyAla][BF_4] and IP of [2PyAla][ClO_4] crystals compared to the OOP response of the periodically poled $LiNbO_3$ sample. Note that d_{15} and d_{33} stand for the IP and OOP piezoresponse.

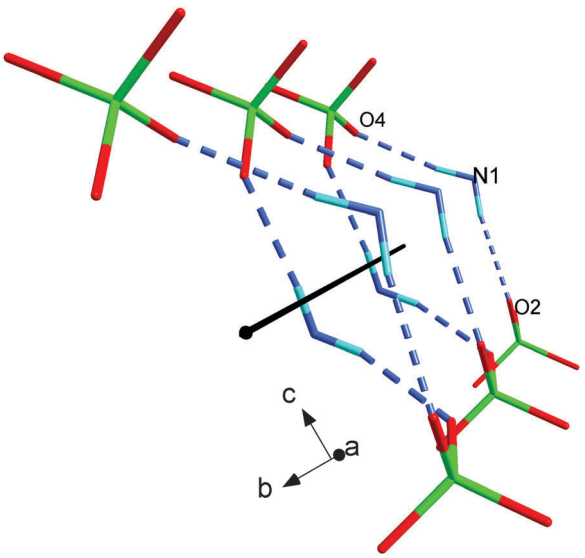

Fig. 7 The spiral chain created by the protonated *H*-β-(2-pyridyl)alanine and perchlorate oxygen ions.

biologically active molecules. In this account it is not attempted to predict the suitable structures which satisfy these demands; however, it appears to be advisable to widen the scope of research into other amino acid–inorganic acid hybrid compositions.

Acknowledgements

MW acknowledges the support of a fellowship ''Development of the potential and educational offer of the University of Wrocław – the chance to enhance the competitiveness of the University'' from the University of Wrocław. Part of this work was developed in the scope of Project CICECO-Aveiro Institute of Materials (ref. FCT UID/CTM/50011/2013), financed by national funds through the FCT/MEC and, when applicable, cofinanced by FEDER under the PT2020 Partnership Agreement. This work was partly supported by the Government of the Russian Federation (Act 211, Agreement 02.A03.21.0006).

References

1 *Piezoelectric and Acoustic Materials for Transducers Applications*, ed. A. Safari and K. Akdogan, Springer, New York, 2008.
2 A. J. Lovinger, *Science*, 1983, **220**, 1115.
3 S. Das and J. Appenzeller, *Nano Lett.*, 2011, **11**, 4003.
4 R. C. G. Naber, C. Tanase, P. W. M. Blom, G. H. Gelinck, A. W. Marsman, F. J. Touwslager, S. Setayesh and D. M. Leeuw, *Nat. Mater.*, 2005, **4**, 243.
5 A. Piecha, A. Gągor, R. Jakubas and P. Szklarz, *CrystEngComm*, 2013, **15**, 940.
6 S. Horiuchi and Y. Tokura, *Nat. Mater.*, 2008, **7**, 357.
7 E. Gazit, *FASEB J.*, 2002, **16**, 77.
8 C. H. Görbitz, *Chem. – Eur. J.*, 2001, **7**, 5153.
9 C. H. Görbitz, *New J. Chem.*, 2003, **27**, 1789.
10 C. H. Görbitz, *Chem. Commun.*, 2006, 2332.
11 E. Gazit, *Chem. Soc. Rev.*, 2007, **36**, 1263.
12 M. Reches and E. Gazit, *Curr. Nanosci.*, 2006, **2**, 105.
13 V. L. Sedman, L. Adler-Abramovich, S. Allen, E. Gazit and S. J. B. Tendler, *J. Am. Chem. Soc.*, 2006, **128**, 6903.
14 N. Kol, L. Adler-Abramovich, D. Barlam, R. Z. Shneck, E. Gazit and I. Rousso, *Nano Lett.*, 2005, **5**, 1343.
15 A. Kholkin, N. Amdursky, I. Bdikin, E. Gazit and G. Rosenman, *ACS Nano*, 2010, **4**, 610.
16 E. D. Bosne, A. Heredia, S. Kopyl, D. V. Karpinsky, A. G. Pinto and A. L. Kholkin, *Appl. Phys. Lett.*, 2013, **102**, 073504.
17 M. Fleck and A. M. Petrosyan, *Salts of Amino Acids*, Springer International Publishing, 2014.
18 W. Bi and N. Mercier, *Chem. Commun.*, 2008, 5743–5745.
19 R. A. Ganeev, *Nonlinear Optical Properties of Materials*, Springer, Berlin, Heidelberg, New York, 2000.
20 R. Surekha, R. Gunaseelan, P. Sagayaraj and K. Ambujam, *CrystEngComm*, 2014, **16**, 7979.
21 S. Parsons, H. Flack and T. Wagner, *Acta Crystallogr., Sect. B: Struct. Sci., Cryst. Eng. Mater.*, 2013, **69**, 249–259.
22 A. Kholkin, S. V. Kalinin, A. Roelofs and A. Gruverman, in *Scanning Probe Microscopy: Electrical and Electromechanical Phenomena at the Nanoscale*, ed. S. V. Kalinin and A. Gruverman, Springer New York, New York, NY, 2007, ch. Review of Ferroelectric Domain Imaging by Piezoresponse Force Microscopy, pp. 173–214.
23 *CrysAlisCCD CrysAlis RED, Version 1.171.33.42, release 29-05-2009 CrysAlis171*, 2009.
24 CrysAlisPro, Agilent Technologies, Version 1.171.37.35h, release 09-02-2015.
25 G. M. Sheldrick, *Acta Crystallogr., Sect. A: Found. Crystallogr.*, 2008, **64**, 112–122.
26 S. K. Seth, I. Saha, C. Estarellas, A. Frontera, T. Kar and S. Mukhopadhyay, *Cryst. Growth Des.*, 2011, **11**, 3250–3265.
27 S. K. Seth, *CrystEngComm*, 2013, **15**, 1772–1781.
28 S. K. Seth, V. S. Lee, J. Yana, S. M. Zain, A. C. Cunha, V. F. Ferreira, A. K. Jordao, M. C. B. de Souza, S. M. S. Wardell,

J. L. Wardell and E. R. T. Tiekink, *CrystEngComm*, 2015, **17**, 2255–2266.
29 C. Etter, J. C. MacDonald and J. Bernstein, *Acta Crystallogr., Sect. B: Struct. Sci.*, 1990, **46**, 256–262.
30 T. Steiner and G. Desiraju, *Chem. Commun.*, 1998, 891–892.
31 D. D. Hadži and S. Bratos, *The Hydrogen Bonds. Recent Developments in Theory and Experiments. [in] Vibrational Spectroscopy of the Hydrogen Bond*, North-Holland, Amsterdam, 1976, vol. 2.
32 L. L. Samorjai and D. Hornig, *J. Chem. Phys.*, 1980, **1962**, 36.
33 G. Bator and L. Sobczyk, *Wiad. Chem.*, 2011, **65**, 869–885.
34 S. Kumar, A. K. Rai, S. Rai, D. Rai, A. Singh and V. Singh, *J. Mol. Struct.*, 2006, **791**, 23–29.
35 M. Kątcka and T. Urbański, *Bull. Acad. Pol. Sci., Ser. Sci. Chim.*, 1964, **XII**, 615.
36 M. Wojtaś, G. Bator and J. Baran, *Vib. Spectrosc.*, 2003, **15**, 5765–5781.
37 R. J. Acheson and P. W. M. Jacobs, *J. Phys. Chem.*, 1970, **74**, 281.
38 D. A. B. M. M. Markowitz and J. H. Stewart, *J. Phys. Chem.*, 1964, **68**, 2282.
39 M. Abplanalp, L. M. Eng and P. Günter, *Appl. Phys. A: Mater. Sci. Process.*, 1998, **66**, S231–S234.
40 J. F. Nye, *Physical Properties of Crystals. Their Representation by Tensors and Matrices*, Clarendon press, 1957.
41 M. Wojtaś, A. Gągor and A. L. Kholkin, *J. Mol. Struct.*, 2014, **1075**, 213–219.
42 S. V. Kalinin, A. Rar and S. A. Jesse, *IEEE Trans. Ultrason., Ferroelectr. Freq. Control*, 2008, **53**, 2226–2252.
43 E. A. Eliseev, S. V. Kalinin and S. Jesse, *J. Appl. Phys.*, 2007, **102**, 014109.
44 *Properties of Lithium Niobate*, ed. K. K. Wong, INSPEC, The Institution of Electrical Engineers, London, United Kingdom, 2002.
45 S. W. Wukovitz and T. O. Yeates, *Nat. Struct. Biol.*, 1995, **2**, 1062–1067.
46 T. O. Yeates and S. B. Kent, *Annu. Rev. Biophys.*, 2012, **41**, 41–61.
47 J. R. Granja and M. R. Ghadiri, *J. Am. Chem. Soc.*, 1994, **116**, 10785–10786.
48 M. Wojtaś, A. Bil, A. Gągor, W. Medycki and A. L. Kholkin, *CrystEngComm*, 2016, **18**, 2413.
49 A. M. Petrosyan, Formation Mechanisms of Nonlinear Optical Crystalline Salts of L-Arginine and L-Histidine, *Proceedings of conference on "Laser Physics-2003"*, Ashtarak, 2004, p. 148.
50 S. B. Monaco, L. E. Davis, S. P. Velsko, F. T. Wang, D. Eimerl and A. Zalkin, *J. Cryst. Growth*, 1987, **85**, 252.
51 S. S. Terzyan, H. A. Karapetyan, R. B. Sukiasyan and A. M. Petrosyan, *J. Mol. Struct.*, 2004, **687**, 111–117.
52 Kirk-Othmer Encyclopedia of Chemical Technology, 4th edn, Volumes: New York, NY. J, 1991-Present., p. (1994), John Wiley and Sons, New York, NY, 4th edn, 1994, vol. 1.
53 A. S. Tayi, A. Kaeser, M. Matsumoto, T. Aida and S. I. Stupp, *Nat. Chem.*, 2015, **7**, 281.
54 S. Garain, T. K. Sinha, P. Adhikary, K. Henkel, S. Sen, S. Ram, C. Sinha, D. Schmeißer and D. Mandal, *ACS Appl. Mater. Interfaces*, 2015, **7**, 1298–1307.
55 S. Jana, S. Garain, S. Sen and D. Mandal, *Phys. Chem. Chem. Phys.*, 2015, **17**, 17429–17436.
56 M. M. Alam and D. Mandal, *ACS Appl. Mater. Interfaces*, 2016, **8**, 1555–1558.
57 A. Tamang, S. K. Ghosh, S. Garain, M. M. Alam, J. Haeberle, K. Henkel, D. Schmeisser and D. Mandal, *ACS Appl. Mater. Interfaces*, 2015, **7**, 16143–16147.